SIMULATION OF THE DYNAMICS OF PLASMA EXPANSION, THE FORMATION AND INTERACTION OF SHOCK AND HEAT WAVES IN THE GAS AT THE NANOSECOND LASER IRRADIATION

P. V. BRESLAVSKIY[1], A V. MAZHUKIN[1,2], O. N. KOROLEVA[1,2]

[1]Keldysh Institute of Applied Mathematics Russian Academy of Sciences
Miusskaya sq., 4, Moscow, 125047, Russia. e-mail: vim@modhef.ru

[2]National Research Nuclear University MEPhI

Summary. The structure of shock and heat waves in the air, caused by the spread of laser plasma at the nanosecond exposure mode is studied by methods of mathematical modeling. The simulation showed that for nanosecond laser pulses, the formation of plasma occurs during the pulse, and the changes in the structure of the plasma torch, plasma expansion features, occurrence of shock and thermal waves depend on a number of parameters and the impact properties of the environment. The nature of the interaction of thermal and hydrodynamic flow quality varies with the magnitude of the thermal conductivity of the medium. The high thermal conductivity of the medium gives rise to thermal waves of two different types - the supersonic and subsonic. The structure of the solutions of supersonic mode is represented as two consecutive waves - thermal and hydrodynamic. The structure of the solutions in the subsonic mode is much more complicated and is represented in the form of three waves following each other - supersonic thermal wave, isothermal shock wave and the subsonic thermal wave coming after the shock. To solve nonlinear equations of hydrodynamics with a thermal conductivity finite-difference approach is used, combined with the procedure of dynamic adaptation of the computational grid, allowing explicitly tracking the strong (shock waves) and weak (thermal wave front) discontinuities.

1 INTRODUCTION

Pulsed laser impact on material has numerous applications, some of which is based on the laser ablation. Laser ablation is a complex phenomenon involving many interrelated processes occurring both during and after laser irradiation. Applications such as pulsed laser deposition (PLD)[1], a laser-induced breakdown spectroscopy (LIBS)[2,3], laser ablation with inductively coupled plasma of mass spectrometry (LA-ICP-MS)[4], production of nanomaterials[5,6], radiation sources for lithography[7], radiation sources of hard ultraviolet and soft X-ray[8, 9], and others based on the laser ablation.

So many applications of pulsed laser impact make it an attractive direction for fundamental research. Despite the fact that there were carried out extensive fundamental investigations of laser-plasma torches 10.11, the basic propositions of the physics of pulsed laser ablation (PLA) were not fully understood because of the complex processes of interaction of laser radiation and plasma with the vaporized material and the environment. Many previous experimental and theoretical works were focused on the study of the adiabatic expansion of a laser plasma in a vacuum, despite the fact that most applications of PLA performed in the presence of ambient gas[12]. The presence of external gas environment sharply changes the

2010 Mathematics Subject Classification: 00A72, 35L67, 35Q31, 76L05, 76N15.
Key words and Phrases: Laser Plasma Processes, Nonlinear Heat Conductivity, Hydrodynamic Simulation, Dynamic Adaptation Method.

mode of the laser impact on the target, changes the conditions of the appearance of laser plasma and increases the complexity of the description of the process of laser ablation due to changing the structure of the plasma torch, special aspects of expansion of the plasma and appearance of shock wave[13-15].

Characteristics of laser-plasma formations depend on many parameters, such as target material[16, 17,18] wavelength, laser pulse duration[19,20], intensity[21], ambient pressure[13,22] and gas composition[23]. The underlying physical mechanisms of material ablation different for nanosecond (ns) and femtosecond (fs) laser pulses[24,25]. For laser pulses of femto-picosecond duration process of formation of plasma transformations occur after the laser pulse ending[24,26]. In ablation dominated homogeneous mechanisms of phase transformations and related spallation phenomena[27-29].

For a nanosecond laser pulses the process of formation of plasma occurs during the pulse and is interconnected with the process of material ablation. In ablation dominant role usually played by the processes of heat conduction and heterogeneous mechanisms of phase transitions (melting, evaporation) and the impact of a laser plasma formed in a gas medium. At a certain ratio of the parameters of the laser influence can be realized fast ablation modes based on the processes of explosive boiling and spinodal decomposition of overheated liquid phase[30,31]. Interaction of laser radiation of nanosecond duration with a torch can be significant. The resulting plasma can absorb and scatter laser radiation therewith screening the surface of the target, reducing the effectiveness of the ablation of materials. Highly heated plasma can also reemit absorbed energy in a shorter wavelength range, increasing the effectiveness of the ablation. For this reason, nanosecond laser ablation continues to be an active area of comprehensive studies[32,33]. The purpose of this paper is to study the structure of shock and heat waves in the air, caused by the propagating of laser plasma at the nanosecond influence mode.

2 STATEMENT OF THE PROBLEM AND BASIC ASSUMPTIONS

On a metal target placed in a gas (air) environment from right to left falls the flux of laser radiation, Fig.1. Incident flux $G(t) = G_0\ (0.5\tau_o - |0.5\tau_o - t|)^{1/2}$, is partially absorbed $A \cdot G(t)$, causing heating and evaporation of the target, where τ_o - duration of the laser pulse, A - absorptivity of surface. Another part of the flux $(1-A) \cdot G(t)$, is mirrored. Evaporated material, heating and ionizing under the influence of laser flux, expands and effect push out action on the cold ambient gas.

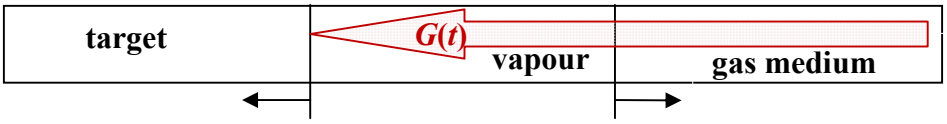

Fig. 1. Scheme of problem under research.

In problems of gas dynamics describing the spread of high-temperature laser plasma, the basic mechanisms of energy transfer, along with radiation, are convective and conductive. Basis of mathematical models, in this case, together with the radiative transfer equation, constitute the equations of hydrodynamics with nonlinear thermal conductivity. Previously it paid great attention to the influence of nonlinear thermal conductivity on the peculiarities of

interaction of thermal processes with hydrodynamic[34,35]. It was found that solutions of this class of problems is a great variety, and within a relatively narrow range of parameters can be realized self-similar solutions[36], widely used for testing numerical solutions.

From the computational point of view the solution of hydrodynamic equations with nonlinear thermal conductivity refers to the problems of high complexity. A typical solution to these problems is complex structure and includes strong (shock wave front) and weak (thermal wave front) breaks, zones of large gradients of temperature, pressure, density and velocity. The structure of shock wave front and the thermal wave front depends on the degree of nonlinearity of thermal conductivity equation. Excluding the dissipative processes in the medium shock wave is strong discontinuity of all solution components u, ρ, P, T. Consideration of thermal conductivity eliminate discontinuity of function $T(x,t)$ and leads to the appearance of the effective width of the front in temperature. At low thermal conductivity shock wave front by a temperature close to quasi-discontinuous. Strong thermal conductivity of the medium (power dependence of the thermal conductivity from temperature), which is characteristic for a fully ionized plasma, results in a significant increase in the effective width of the shock wave front and in appearance of temperature waves, which front at the tie point of the solution to the undisturbed background is a weak discontinuity.

The presence of discontinuous solutions, areas of high gradients and their rapid propagation in space presents stringent requirements on the effectiveness of used computing algorithms, first of all, not so much to the quality of difference schemes as to the principles of construction of optimal computational grids.

In order to significantly simplify the statement of the problem it is proposed to exclude from consideration process of target evaporation, assuming that at time $t=t_0$ near the evaporating surface was formed a thin layer of plasma $T(0,t_0)=T_0$, $\rho(0, t_0) = \rho_0$, front of which propagates at the speed $u(0, t)=u_0(t)$. It is assumed that the laser flux is completely absorbed on the plasma front, plasma is fully ionized, which allows to describe the radiative transport in the approximation of radiant thermal conductivity.

Mathematical statement of the problem. Statement of the problem of laser plasma spread in a gaseous medium is described in the Euler variables in one-dimensional non-stationary problem of hydrodynamics with nonlinear thermal conductivity:

$$\begin{gathered}\frac{\partial \rho}{\partial t}+\frac{\partial}{\partial x}(\rho u)=0 \\ \frac{\partial}{\partial t}(\rho u)+\frac{\partial}{\partial x}(P+\rho u^2)=0 \\ \frac{\partial}{\partial t}(\rho \varepsilon)+\frac{\partial}{\partial x}(\rho u \varepsilon)+P\frac{\partial u}{\partial x}+\frac{\partial W}{\partial x}=0 \\ W=-\lambda(T,\rho)\frac{\partial T}{\partial x}\end{gathered} \tag{2.1}$$

with the equations of state

$$P=\rho RT,\ \ \varepsilon=\frac{R}{\gamma-1}T.$$

Here, ρ is the density, u is the velocity, P is the pressure, ε is the internal energy, T is the temperature, R is the gas constant, γ is the adiabatic index, W is heat flux, and λ is the thermal conductivity. It is assumed that λ is a power function of the temperature and density[37]: $\lambda(T, \rho) = \lambda_\circ T^a \rho^b$.

Initial conditions. At the initial time $t = t_0$ is assumed zero background of velocity and constant by the space density and temperature:

$$u(x, t_0) = 0, \;\; T(x, t_0) = \mathrm{T}_0, \;\; \rho(x, t_0) = \rho_0 \tag{2.2}$$

Boundary conditions. Formulation of boundary conditions made taking into account the fact that the left-plane $x = \Gamma_p(t)$ is a surface of plasma front, which at $G \neq 0$ is the source of motion and heating, so on it formulated two boundary conditions that determine the velocity and the magnitude of heat flux:

$$u\big(\Gamma_p(t), t\big) = v_0(0.5\tau_0 - |0.5\tau_0 - t|)^n,$$
$$G\big(\Gamma_p(t), t\big) = W\big(\Gamma_p(t), t\big) = \rho_0 {v_0}^3(0.5\tau_0 - |0.5\tau_0 - t|)^{3n} \tag{2.3}$$

The particular values of a, b, and n will be specified later. The background values are preserved on the right boundary $x = \infty$:

$$u(\infty, t) = 0, \qquad T(\infty, t) = T_0, \qquad \rho(\infty, t) = \rho_0 \tag{2.4}$$

Relations on the shock front. Since the temperature across the front shock $x = \Gamma_W(t)$ is continuous, we write three conservation laws (Rankine–Hugoniot relations):

$$\rho_-(u_- - v_W) = \rho_+(u_+ - v_W) = D_M$$
$$P_- + \rho_-(u_- - v_W)^2 = P_+ + \rho_+(u_+ - v_W)^2$$
$$\varepsilon_- + \frac{P_-}{\rho_-} + \frac{(u_- - v_W)^2}{2} + \frac{W_-}{D_M} = \varepsilon_+ + \frac{P_+}{\rho_+} + \frac{(u_+ - v_W)^2}{2} + \frac{W_+}{D_M} \tag{2.5}$$

Here, the minus and plus indices denote the variables on different sides of the shock wave, v_W is the velocity of the shock wave, and D_M is the mass flux across the shock front.

3 DYNAMIC ADAPTATION METHOD

Solution of nonlinear equations of hydrodynamics with a thermal conductivity (2.1) is carried out by finite-difference schemes, combined with the procedure of dynamic adaptation of the computational grid. The principles of construction of computing finite-difference algorithms with dynamic adaptation for a wide class of equations of parabolic and hyperbolic types with moving and fixed boundaries presented in detail in[38-41]. It also contains cited literature on methods of adaptation.

An arbitrary non-stationary coordinate system. According to the dynamic adaptation method we make transition to an arbitrary non-stationary coordinate system. In the new variables (q, τ), system (2.1) becomes

$$\frac{\partial}{\partial \tau}(\psi\rho) + \frac{\partial}{\partial q}\big(\rho(u + Q)\big) = 0 \tag{3.1}$$

$$\frac{\partial}{\partial\tau}(\psi\rho u)+\frac{\partial}{\partial q}\big(P+\rho u(u+Q)\big)=0 \tag{3.2}$$

$$\frac{\partial}{\partial\tau}(\psi\rho\varepsilon)+\frac{\partial}{\partial q}\big(\varepsilon\rho(u+Q)\big)+P\frac{\partial u}{\partial q}+\frac{\partial W}{\partial q}=0,\ \ W=-\frac{\lambda(T,\rho)}{\psi}\frac{\partial T}{\partial q} \tag{3.3}$$

$$\frac{\partial\psi}{\partial\tau}=-\frac{\partial Q}{\partial q}, \tag{3.4}$$

where ψ is the Jacobian of the inverse transformation and Q is the adaptation function to be determined.

Taking into account that all perturbations occur on the left boundary (surface of the plasma front) $x=\Gamma_p(t)$ and propagate in the direction to the right one, in order to save computational resources it is advisable to exclude from consideration the area not covered by perturbation. For this purpose the right boundary is shifted to the left and is located at a small distance from it. At the time of appearance the perturbation on the right boundary it is declared free boundary $x=\Gamma_T(t)$ and propagates with a velocity of heat or gas-dynamic perturbations. The new boundary $x=\Gamma_T(t)$ in a nonlinear thermal conductivity problems with a non-zero temperature background will always with the time come closer to the temperature wave front. The propagation velocity of the gas-dynamic perturbations v_T determined by the ratio derived from the equation of motion in the moving coordinate system. The other conditions are transferred from (2.4) unchanged:

$$x=\Gamma_T(t):\qquad v_T=\frac{1}{\rho_0}\frac{\partial P}{\partial u},\ \ u(\Gamma_T(t),t)=0,\ \ T(\Gamma_T(t),t)=T_0,\ \ \rho(\Gamma_T(t),t)=\rho_0$$

Thus, on proceeding to an arbitrary non-stationary coordinate system, the original differential model (2.1) is transformed into extended model (3.1)–(3.4), which has been supplemented by the inverse transformation equation (3.4). Accordingly, the necessary additions are introduced in initial (2.2) and boundary (2.3)–(2.5) conditions:

$$\tau=0:\qquad u(q,0)=0,\ \ T(q,0)=T_0,\ \ \rho(q,0)=\rho_0 \tag{3.5}$$

$$q=\Gamma_P:\qquad u\big(\Gamma_p,\tau\big)=v_0(0.5\tau_0-|0.5\tau_0-\tau|)^n,$$
$$G\big(\Gamma_p,\tau\big)=W\big(\Gamma_p,\tau\big)=v_0{}^3(0.5\tau_0-|0.5\tau_0-\tau|)^{3n}, \tag{3.6}$$
$$Q\big(\Gamma_p,\tau\big)=-v_0(0.5\tau_0-|0.5\tau_0-\tau|)^n$$

$$q=\Gamma_T:\qquad u(\Gamma_T,\tau)=0,\ \ T(\Gamma_T,\tau)=T_0,\ \ Q(\Gamma_T,\tau)=-\frac{1}{\rho_0}\frac{\partial P}{\partial u},\ \ \rho(\Gamma_T,\tau)=\rho_0 \tag{3.7}$$

In the non-stationary coordinate system discontinuities are explicitly introduced in the solution and after a shock wave appears, system (3.1)–(3.4) is solved in two subdomains divided by the shock front. At the front, the resulting solutions are joined using the Rankine–Hugoniot conditions:

$$q=\Gamma_W:\qquad \rho_-(u_-+Q_W)=\rho_+(u_++Q_W)=D_M \tag{3.8}$$

$$P_- + \rho_-(u_- + Q_W)^2 = P_+ + \rho_+(u_+ + Q_W)^2$$

$$W_- + 0.5\rho_-(u_- + Q_W)^3 = W_+ + 0.5\rho_+(u_+ + Q_W)^3$$

$$Q_W = -v_W$$

4 FINITE DIFFERENCE APPROXIMATION

System (3.1)–(3.8) was numerically solved on the grid:

$$\omega_{h,\Delta\tau} = \left\langle \begin{matrix}(q_i, \tau^j), (q_{i+1/2}, \tau^j), \;\; q_{i+1} = q_i + h, q_{i+1/2} = q_i + 0.5h, i = 0,1,\dots,N-1 \\ \tau^{j+1} = \tau^j + \Delta\tau^j, \;\; j = 0,1,\dots \end{matrix} \right\rangle.$$

The differential equations were approximated by finite differences on staggered grids. Specifically, we used the following family of difference schemes, in which the density $\rho_{i+1/2}$, the temperature $T_{i+1/2}$, the pressure $P_{i+1/2}$, and the internal energy $\varepsilon_{i+1/2}$ were determined at the half-integer points, while the velocity u_i and the function Q_i were determined at the integer points:

$$\frac{\psi_{i+\frac{1}{2}}^{j+1} - \psi_{i+\frac{1}{2}}^{j}}{\Delta\tau^j} = -\frac{Q_{i+1}^{\sigma_1} - Q_i^{\sigma_1}}{h_{i+\frac{1}{2}}}$$

$$\frac{\psi_{i+\frac{1}{2}}^{j+1}\rho_{i+\frac{1}{2}}^{j+1} - \psi_{i+\frac{1}{2}}^{j}\rho_{i+\frac{1}{2}}^{j}}{\Delta\tau^j} = -\frac{\rho_{i+1}^{\sigma_2}\left(u_{i+1}^{\sigma_3} + Q_{i+1}^{\sigma_1}\right) - \rho_i^{\sigma_2}\left(u_i^{\sigma_3} + Q_i^{\sigma_1}\right)}{h_{i+\frac{1}{2}}}$$

$$\frac{\psi_i^{j+1}\rho_i^{j+1}u_i^{j+1} - \psi_i^j\rho_i^j u_i^j}{\Delta\tau^j} =$$

$$= -\frac{P_{i+\frac{1}{2}}^{\sigma_4} - P_{i-\frac{1}{2}}^{\sigma_4} + \rho_{i+\frac{1}{2}}^{\sigma_2}u_{i+\frac{1}{2}}^{\sigma_3}\left(u_{i+\frac{1}{2}}^{\sigma_3} + Q_{i+\frac{1}{2}}^{\sigma_1}\right) - \rho_{i-\frac{1}{2}}^{\sigma_2}u_{i-\frac{1}{2}}^{\sigma_3}\left(u_{i-\frac{1}{2}}^{\sigma_3} + Q_{i-\frac{1}{2}}^{\sigma_1}\right)}{0.5\left(h_{i+\frac{1}{2}} + h_{i-\frac{1}{2}}\right)} \tag{4.1}$$

$$\frac{\psi_{i+\frac{1}{2}}^{j+1}\rho_{i+\frac{1}{2}}^{j+1}\varepsilon_{i+\frac{1}{2}}^{j+1} - \psi_{i+\frac{1}{2}}^{j}\rho_{i+\frac{1}{2}}^{j}\varepsilon_{i+\frac{1}{2}}^{j}}{\Delta\tau^j} =$$

$$= -P_{i+\frac{1}{2}}^{\sigma_4}\frac{u_{i+1}^{\sigma_3} - u_i^{\sigma_3}}{h_{i+\frac{1}{2}}} - \frac{\rho_{i+1}^{\sigma_2}\varepsilon_{i+1}^{\sigma_5}\left(u_{i+1}^{\sigma_3} + Q_{i+1}^{\sigma_1}\right) - \rho_i^{\sigma_2}\varepsilon_i^{\sigma_5}\left(u_i^{\sigma_3} + Q_i^{\sigma_1}\right)}{h_{i+\frac{1}{2}}} +$$

$$+ \frac{\frac{\lambda\left(\rho_{i+1}^{\sigma_2}, T_{i+1}^{\sigma_5}\right)}{\psi_{i+1}^{\sigma_1}}\frac{T_{i+\frac{3}{2}}^{\sigma_5} - T_{i+\frac{1}{2}}^{\sigma_5}}{0.5\left(h_{i+\frac{3}{2}} + h_{i+\frac{1}{2}}\right)} - \frac{\lambda\left(\rho_i^{\sigma_2}, T_i^{\sigma_5}\right)}{\psi_i^{\sigma_1}}\frac{T_{i+\frac{1}{2}}^{\sigma_5} - T_{i-\frac{1}{2}}^{\sigma_5}}{0.5\left(h_{i+\frac{1}{2}} + h_{i-\frac{1}{2}}\right)}}{h_{i+\frac{1}{2}}}$$

Here $f^{\sigma_r} = \sigma_r f^{j+1} + (1-\sigma_r) f^j$, a $\sigma_r = \sigma_1, \sigma_2, \ldots$ are the weighting factors determining the degree to which the difference scheme is implicit. If $\sigma_1 = \sigma_2 = \ldots = 0$, we obtain a completely explicit difference scheme with an $O(\Delta\tau + h^2)$ approximation error. If $\sigma_1 = \sigma_2 = \ldots = 1$, the scheme is completely implicit with the same order of accuracy. In the case of $\sigma_1 = \sigma_2 = \ldots = 0.5$, we have a scheme with an $O(\Delta\tau^2 + h^2)$ approximation error. The computations were performed using the completely implicit difference scheme with $O(\Delta\tau + h^2)$ accuracy.

For the functions $\{u, Q\} = f$ specified at the integer points of ω, their values at the half-integer points were determined by the formula $f_{i+\frac{1}{2}} = 0.5(f_i + f_{i+1})$. Similarly, the values of the functions $\{\psi, \rho, T, P, \varepsilon\} = f$ at the integer points were determined in terms of their values at the half-integer points: $f_i = 0.5\left(f_{i+\frac{1}{2}} + f_{i-\frac{1}{2}}\right)$. The flowchart of the calculation algorithm presented at Fig. 2. The algorithm involves two internal iteration blocks based on Newton's method. The first block solves the difference analogue of the energy equation, while the second block solves the analogues of the continuity equation, the equation of motion, and grid point redistribution equation (the first three equations in (4.1)). Both blocks are included in the external iteration cycle. If the number of external iteration steps in global cycle exceeds 15 or the number of internal iteration steps exceeds 20, the time step is decreased by 10%. If the number of global iteration steps is less than four, the next time step is increased by 1%. The initial value for each unknown grid function is specified as $f^{j+1(0)} = f^j + \left(f^j - f^{j-1}\right)\Delta\tau^j/\Delta\tau^{j-1}$.

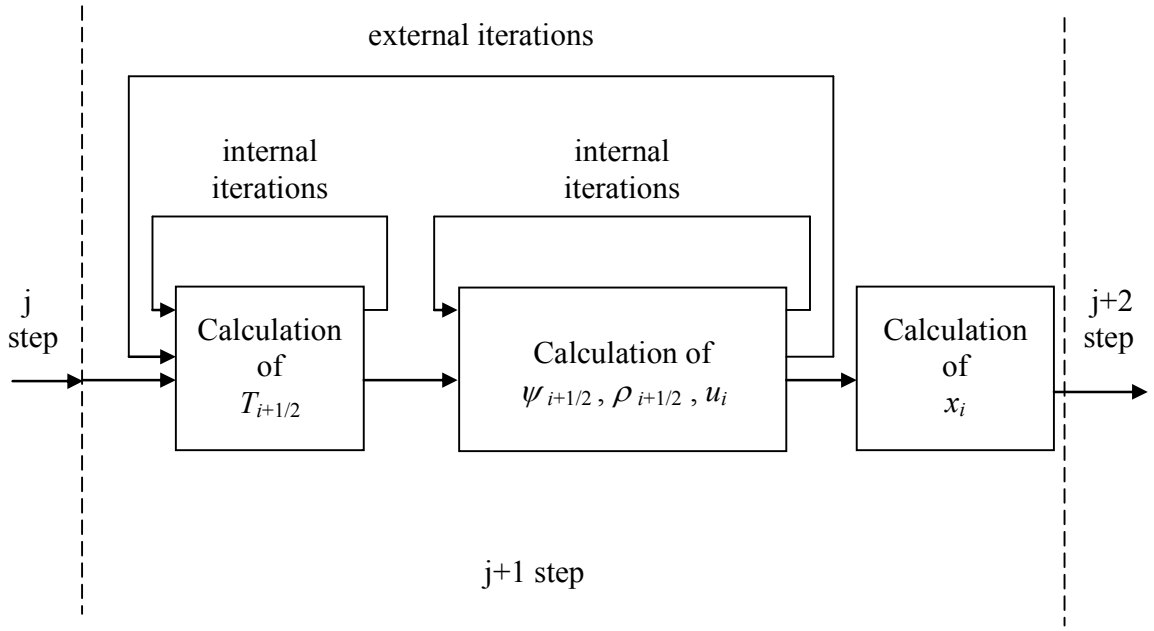

Fig. 2. Flowchart of calculation algorithm.

The Rankine–Hugoniot relations (3.8) are required to hold on the shock wave $q = \Gamma_W$. Since the equations involve six unknowns, three of them are determined by solving system

(3.1)–(3.4) at the boundary points. These are the density ρ_- and the velocity u_- ahead of the shock front and the velocity u_+ behind the shock front. The remaining three unknowns (the shock propagation velocity v_W, the density ρ_+ behind the shock front, and the temperature $T_- = T_+$ on the shock front) are determined by relations (3.8).

5 CHOICE OF THE ADAPTATION FUNCTION

The grid point distribution in the dynamic adaptation method is controlled using the adaptation function Q. In the case of steep-gradient solutions, this function is usually determined from the quasi-stationarity principle[38-42], according to which we choose a nonstationary coordinate system in which all the physical processes proceed as steady-state ones and the corresponding time derivatives are relatively small. Setting the time derivatives in the equations equal to zero yields the sought adaptation function.

The general solution to the complete system of fluid dynamics equations (3.1)–(3.4) is determined by the sum of the velocity, density, and temperature. These functions have different (frequently oppositely directed) spatiotemporal distributions. A controllable grid point distribution for the system of equations must take into account the features of the spatiotemporal distributions for all the solution components.

In the general case, the adaptation function in fluid dynamics problems can be determined using the entire system of equations[38,41.42]. In this paper, the function Q is found from energy equation (3.3), whose solution depends on the velocity, density, and heat conduction. In nonconservative form, the energy equation is

$$\frac{\partial \varepsilon}{\partial \tau} + \frac{(u+Q)}{\psi}\frac{\partial \varepsilon}{\partial q} + \frac{P}{\rho\psi}\frac{\partial u}{\partial q} + \frac{1}{\rho\psi}\frac{\partial W}{\partial q} = 0$$

Based on the quasi-stationarity principle, we set $\partial\varepsilon/\partial\tau = 0$ to obtain the equation

$$\rho(u+Q)\frac{\partial \varepsilon}{\partial q} + P\frac{\partial u}{\partial q} + \frac{\partial W}{\partial q} = 0 \qquad (5.1)$$

By taking into account the particular form of the equations of state $P = \rho RT$, $\varepsilon = \frac{R}{\gamma-1}T$ and differentiating the heat flux $W = -\frac{\lambda(T,\rho)}{\psi}\frac{\partial T}{\partial q}$ the function Q is determined by simple rearrangements in Eq.(5.1):

$$Q = -\left[u + (\gamma-1)T\,\frac{\partial u}{\partial q}\Big/\left(\frac{\partial T}{\partial q} + re\right)\right] +$$
$$+\left[\frac{(\gamma-1)}{R\rho\psi}\left(\frac{\partial \lambda}{\partial \rho}\frac{\partial \rho}{\partial q} + \frac{\partial \lambda}{\partial T}\frac{\partial T}{\partial q} + \lambda(\rho,T)\frac{\partial^2 T}{\partial q^2}\Big/\left(\frac{\partial T}{\partial q} + re\right)\right)\right] + \qquad (5.2)$$
$$+\left[\frac{(\gamma-1)}{R}\frac{\lambda(\rho,T)}{\rho}\frac{\partial}{\partial q}\left(\frac{1}{\psi}\right)\right],$$

where re is a regularizing constant that is a lower bound for the derivative as it tends to zero.

After the difference approximation, the first square bracket in (5.2) exerts a contraction effect on the grid points in u and T. The second square bracket takes into account the

influence of nonlinear heat conduction and exerts a contraction effect with respect to ρ and T. The last term is of the diffusion type. If $\lambda(\rho, T) \neq 0$, it has a smoothing effect and, in particular, prevents the intersection of grid point trajectories.

The features of the class of problems under consideration are determined by two factors. The first is that the thermal conductivity is a power function of the temperature. At low temperatures (near zero), since the thermal conductivity is low, the dissipating effect of the diffusion term decreases sharply and may become insufficient for an optimal grid point distribution. The second factor is that the original problem is represented in the form of a free-boundary problem. The original domain may then increase by many orders of magnitude. Accordingly, the values of ψ increase as well, which also strongly reduces the diffusion component. To eliminate these effects, it is reasonable to supplement Q with a function obtained from the diffusion approximation taking into account the presence of moving boundaries:

$$Q = -D\frac{\partial \psi}{\partial q},$$

where D is the diffusivity. Its value is determined by the geometric size of a cell (the mesh size h), by the velocity of the boundary points (v_l, v_r), and by the minimum of the function ($\psi_{\min}$) over the entire domain:

$$D = \frac{h|\max(v_l, v_r)|}{\psi_{\min}}.$$

Additionally, it is reasonable to represent the ratio of two temperature derivatives in Eq. (5.2) in the form of the derivative of a slowly varying logarithmic function:

$$\frac{\partial^2 T}{\partial q^2}\Big/\left(\frac{\partial T}{\partial q} + re\right) = \frac{\partial}{\partial q}\left(\ln\left(\left|\frac{\partial T}{\partial q}\right| + re\right)\right)$$

In view of the features described above, the adaptation function can be finally written as

$$\begin{gathered} Q = -\left[u + (\gamma - 1)T\frac{\partial u}{\partial T}\right] + \\ + \left[\frac{(\gamma - 1)}{R\rho\psi}\left(\frac{\partial \lambda}{\partial \rho}\frac{\partial \rho}{\partial q} + \frac{\partial \lambda}{\partial T}\frac{\partial T}{\partial q} + \lambda(\rho, T)\frac{\partial}{\partial q}\left(\ln\left(\left|\frac{\partial T}{\partial q}\right| + re\right)\right)\right)\right] - \\ - \left[\left(\frac{(\gamma - 1)}{R}\frac{\lambda(\rho, T)}{\rho\psi^2} + D\right)\frac{\partial \psi}{\partial q}\right]. \end{gathered} \tag{5.3}$$

6 SIMULATION RESULTS

Modeling the problem of propagation of the front of a plasma torch in a gaseous medium is to solve the system (3.1) - (3.4) with the initial (3.5) and boundary (3.6), (3.7) conditions, Rankine–Hugoniot relations (3.8) and the function of adaptation (5.3). Due to the specifics of

the problem under consideration at the initial time selected a thin layer of strongly heated (T=*1.5 eV*) air in a monatomic state. The parameters of the problem on ascending part of the motion of the plasma front ($t \le 0.5\tau_o$) agreed with the previously obtained self-similar solution[42] and set by the following values

$$R = 573\ J/(kg\ \text{K}), \qquad \gamma = 5/3, \qquad \rho_0 = 1\ \ kg/m^3,$$
$$v_0 = 4.64\ 10^5\ \ m/s^{7/6}, \quad T_0 = 17450\ \text{K} \sim 1.5\ \text{eV}, \quad \tau_0 = 2.\,10^{-8}\ s,$$
$$n = 1/6, \quad a = 4, \quad b = -2.$$

Figure 3 shows the time dependences of the gas-dynamic velocity and heat flux (2.3), (3.6) on the boundary of the plasma torch taking into account values of the selected parameters of the problem (υ_o, ρ_o, τ_o, n).

The transformation function (5.3), taking into account the specific thermal conductivity dependence on the temperature and density of $\lambda(T, \rho) = \lambda_o T^4 \rho^{-2}$ becomes:

$$Q = -\left[u + (\gamma - 1)T\frac{\partial u}{\partial T}\right] +$$
$$+\left[\frac{(\gamma-1)}{R\rho\psi}\left(-(2\lambda_0 T^4\rho^{-3})\frac{\partial\rho}{\partial q} + (4\lambda_0 T^3\rho^{-2})\frac{\partial T}{\partial q} + \lambda_0 T^4\rho^{-2}\frac{\partial}{\partial q}\left(\ln\left(\left|\frac{\partial T}{\partial q}\right| + re\right)\right)\right)\right] - \quad (6.1)$$
$$-\left[\left(\frac{(\gamma-1)}{R}\frac{\lambda_0 T^4\rho^{-2}}{\rho\psi^2} + D\right)\frac{\partial\psi}{\partial q}\right].$$

The number of nodes N in all variants of calculations is 30, the position of which in all the figures mentioned by markers.

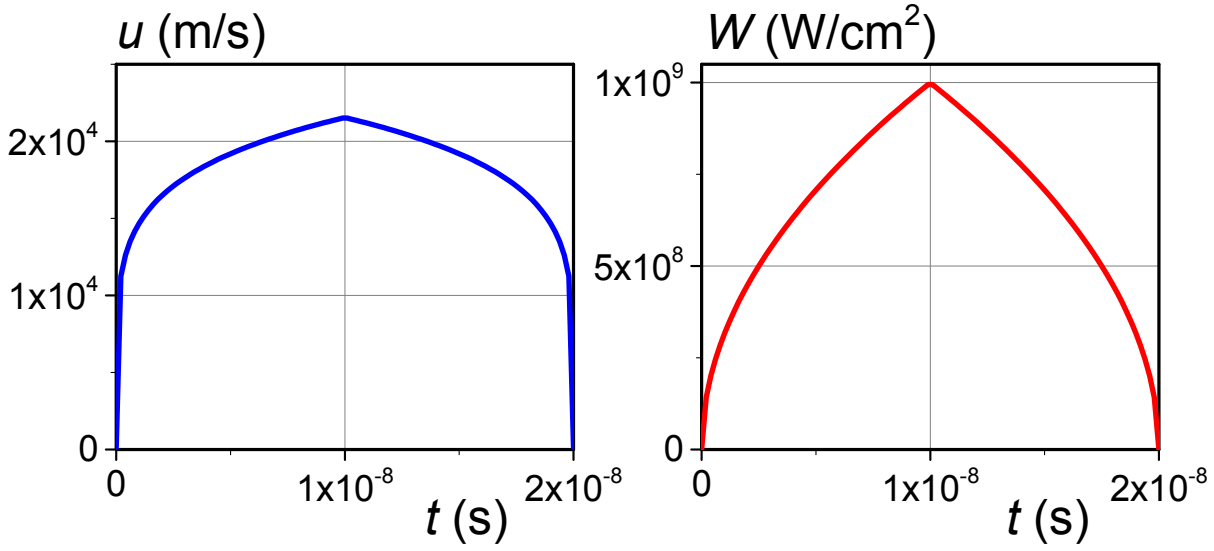

Fig. 3. Time profiles of velocity and flux on the boundary of plasma torch.

One of the purposes of this study is to compare the characteristics of the developing plasma flow depending on the degree of nonlinearity of the thermal processes. The simulation showed that the nature of the interaction of thermal and hydrodynamic fluxes qualitatively varies with the magnitude of the thermal conductivity of the medium. The high thermal conductivity of the medium leads to the appearance temperature waves[35] which are divided into two different types by mode caused by them hydrodynamic motion - supersonic and subsonic. In supersonic regime heat propagates with a finite velocity on the initial background. Behind the front of the supersonic thermal wave appears isothermal shock wave. Temperature wave propagating at subsonic speeds, locates before going in front of it shock wave, and are characterized by equality to zero of heat flux W, by maximum of density ρ and by the local minimum of temperature T.

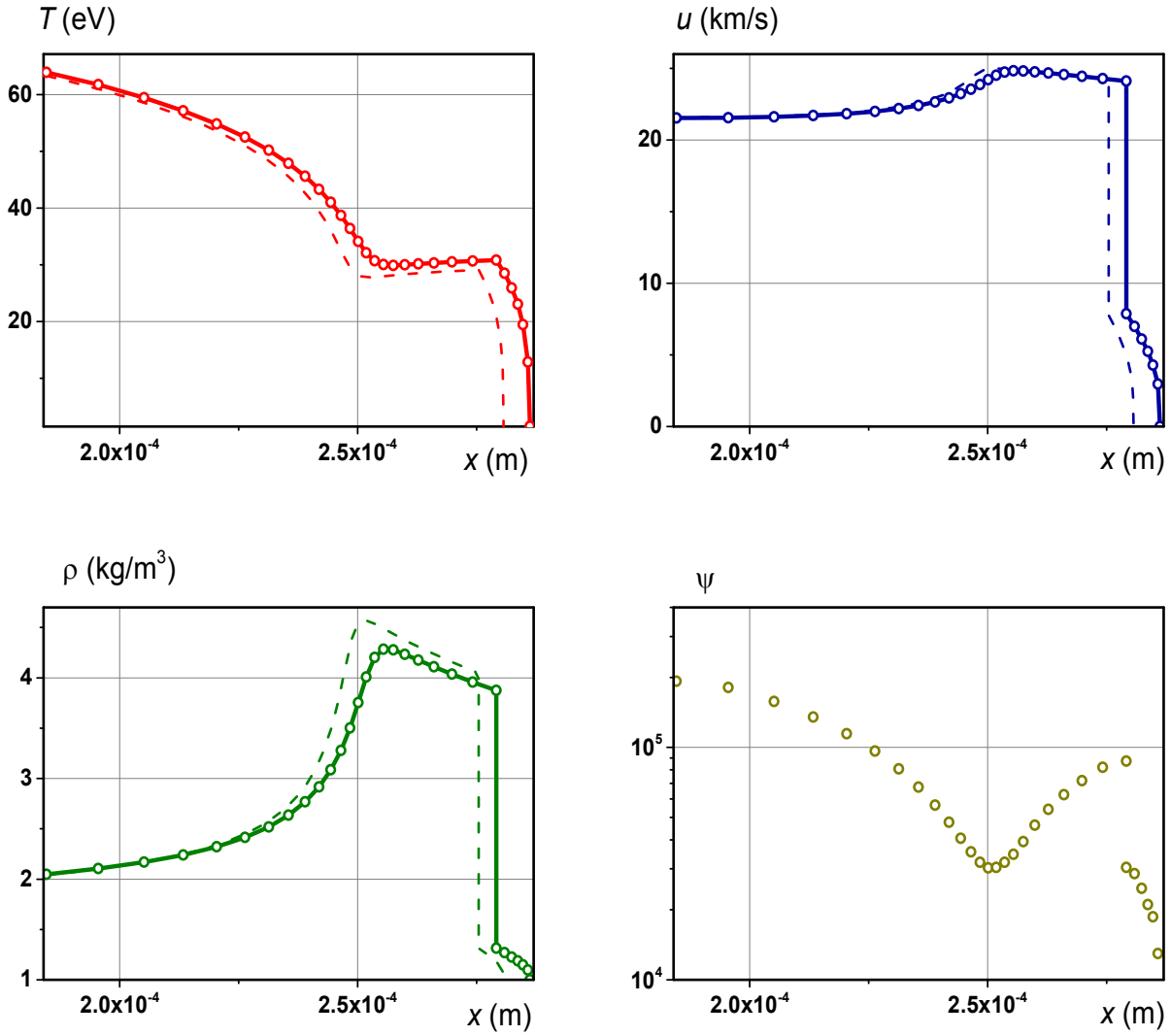

Fig. 4. Subsonic mode with λ_o= 10 at the moment t = 10 ns.

Change of modes of propagation of heat in the case considered depends on the degree of non-linearity of thermal conductivity and determined by value of parameter λ_o. To dimensionless constant λ_o=1 corresponds value of $6.18 \cdot 10^{-24}$ $m^7/(kg \cdot s^3 \cdot K^5)$ (further are values of dimensionless constant λ_o, for certain self-similar modes[42]). At values of λ_o less than a certain value of dimensionless constant λ^* ($\lambda_o < \lambda^*$ for the considered modes $\lambda^* \approx 30$) formed subsonic temperature wave and with reverse ratio $\lambda_o \geq \lambda^*$ there is supersonic temperature wave. In this study, we consider one variant of the subsonic temperature wave with λ_o=10, Fig. 4-5 and two with supersonic λ_o=50 and λ_o=200, Fig. 6-9.

Subsonic mode. Temperature wave with λ_o=10 characterizes the subsonic mode of propagation of heat. After the occurrence of the shock wave 23 nodes fall into the area between the plasma torch and the shock wave, and in the area between the shock wave and external boundary - 7 nodes. Figures 4,5 show the profiles in times t=10 ns and t=20 ns, respectively. The dotted line corresponds to the self-similar solution[42], and a solid line with markers - numerical (markers indicate position of the nodes of the computational grid). Jacobian of inverse transformation characterizes degree of change of the spatial step compared to its initial value. At the moment of occurrence of shock wave flux on the plasma front $G \approx 4. \cdot 10^6$ W/cm^2, the temperature ≈ 30465 K (≈2.63 eV). At t=10 ns flux $G = 1. \cdot 10^9$ W/cm^2, the temperature at the front T≈738600 K (≈63.7 eV). By the end of the calculations at t=20 ns flux and gas-dynamics velocity on the front is equal to zero, the temperature at the front ≈614000 K (≈53 eV).

The structure of the solution in the subsonic mode (Fig. 4,5) is represented in the form of three waves following each other (from right to left):

- supersonic temperature wave generated by the shock wave;
- shock wave which is an isothermal jump with continuous temperature and discontinuous density and velocity;
- subsonic temperature wave going after the shock wave.

At the front of the supersonic temperature wave (weak discontinuity) derivatives of all functions with respect to x are maximal, but, as in the case of only one equation of nonlinear thermal conductivity without taking into account the influence of hydrodynamics, all physical quantities are continuous. At that behind the front heat fluxes, velocity, density and temperature increase sharply.

Shock wave (isothermal discontinuity) is characterized by a strong change of all quantities.

Another area of sharp change of physical quantities is a subsonic temperature wave front. It is characterized by maximum of density, zero heat flux and the local minimum of temperature.

Dimensions of area and spatial grid steps in the physical space characterized by a function $\psi(x,t)$, which is at any given time indicates how many times changed size of step and area as a whole. Taking into account that has been considered region with moving boundaries, in which the velocity of the right border (the front of supersonic temperature wave) far exceeded the the velocity of the left (the front of the plasma), $v_T >> v_p$, the geometric size of the physical area covered by perturbation at the specified time interval increased, according to the curve $\psi(x,t)$, more than 5 orders of magnitude. Local minima of function $\psi(x,t)$ occur in the area of

the largest gradients of solution and coincide with the fronts of subsonic and supersonic temperature waves, Fig. 4,5.

The supersonic mode. In the case of a supersonic temperature wave takes place weak interaction of thermal processes with hydrodynamic. With a strong dependence of the thermal conductivity on temperature and high speed of propagation of heat supersonic mode can become a dominant form of heat transfer.

Figures 6-9 shows the spatial profiles of the gas-dynamic functions of temperature and function ψ for λ_o = 50, 200, respectively. In the calculations was used a grid with the total number of nodes N = 30, the distribution of which noted by markers.

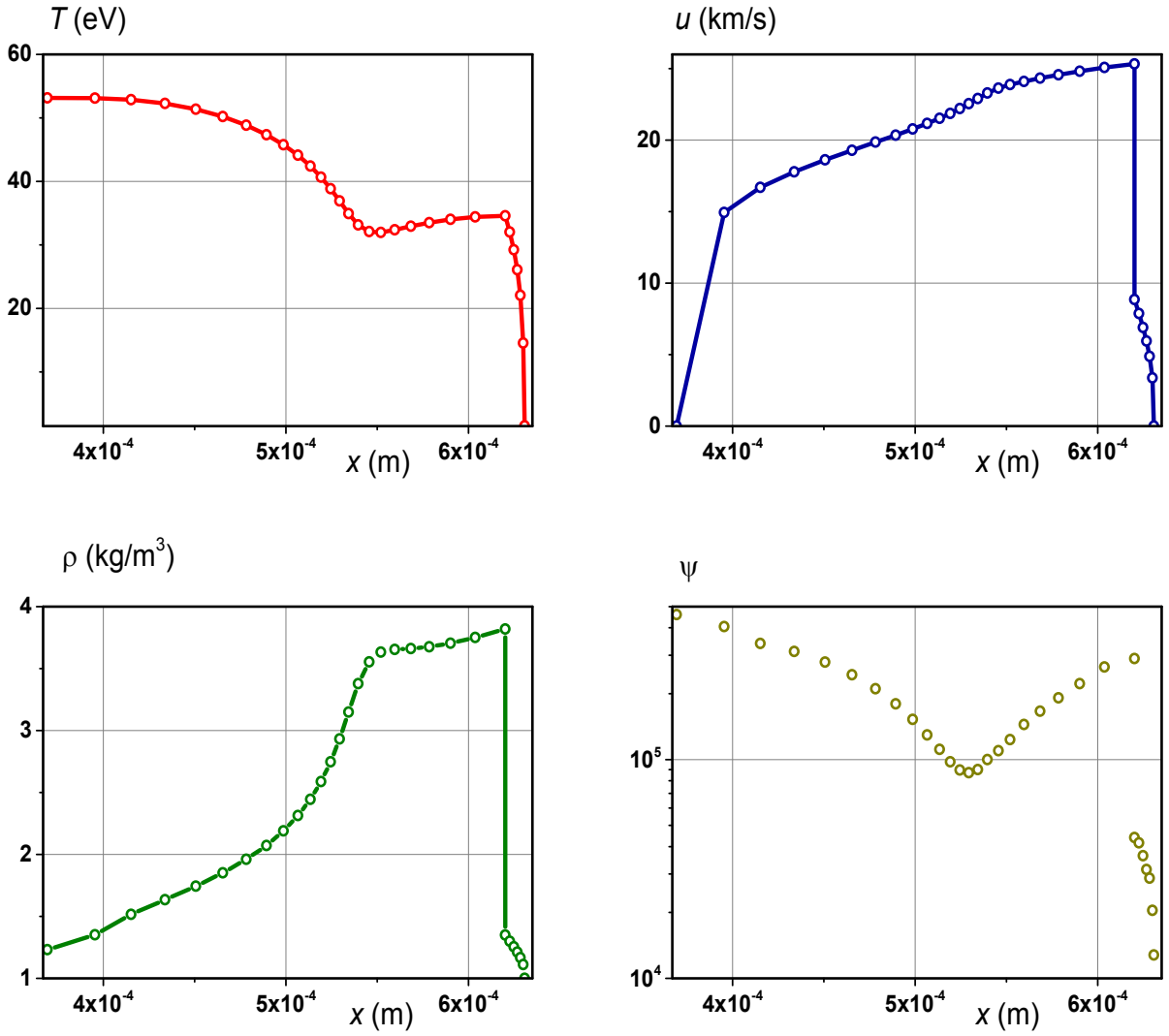

Fig. 5. Subsonic mode with λ_o= 10 at the moment t = 20 ns.

The structure of the solution of supersonic mode is much simpler than subsonic and it can be represented by two following one after another waves - thermal and hydrodynamic. Its propagation velocities in this mode are different, and the temperature wave front is far ahead of the front of hydrodynamic one, Fig. 6-9. Front position in each of them corresponds to a weak and a strong discontinuity, respectively, in the vicinity of which there is the greatest concentration of grid nodes.

In mode with λ_o=50, Fig. 6,7, the temperature wave velocity comparable with that of the shock wave and supersonic heating region is much less than for a medium with a high thermal conductivity (λ_o=200), Fig. 8.9, for which the velocity of propagation of the temperature wave much higher.

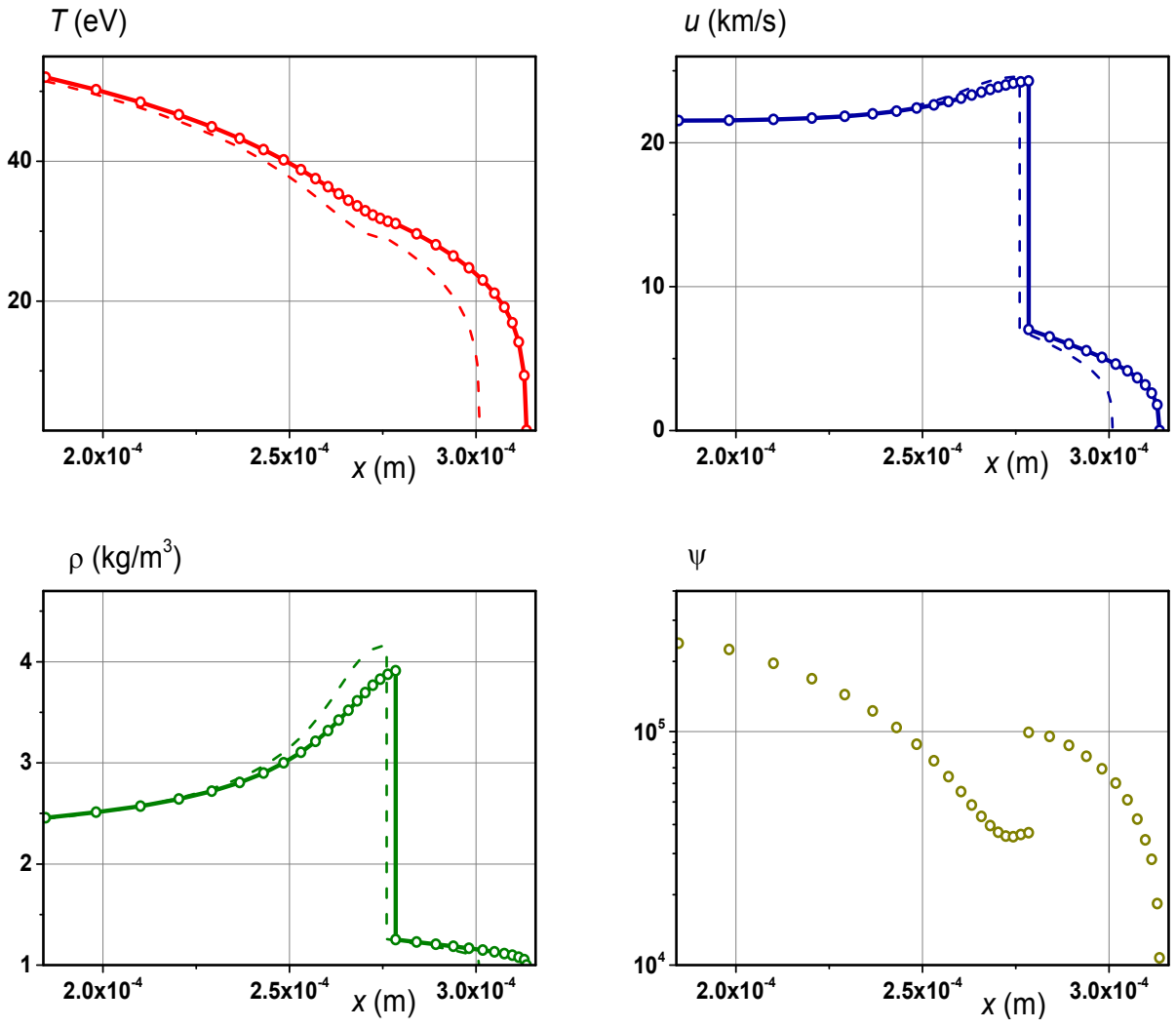

Fig. 6. Supersonic mode with λ_o= 50 at the moment t = 10 ns.

In all of these modes at the moment t=10 ns, Fig. 4,6,8 compared the numerical results obtained (solid line with markers) with the found self-similar solutions for the problem of piston moving at zero temperature background (dashed line)[42]. By now the numerical solution approaches to a self-similar one, which indicates the reliability and quality of the results. The highest temperature achieved at the front of the plasma torch, and as expected, is maximal at a lower thermal conductivity. For λ_o=10 - T_{max}≈64 eV, while for λ_o=200 - T_{max}≈43 eV. By the time t=20 ns (Fig. 5,7,9) gasdynamical velocity and heat flux at the boundary of the plasma torch is equal to zero, which leads to reduction of density on the boundary and to the temperature drop throughout the solution domain. In the future, this should lead to a separation of the area under consideration from the plasma torch.

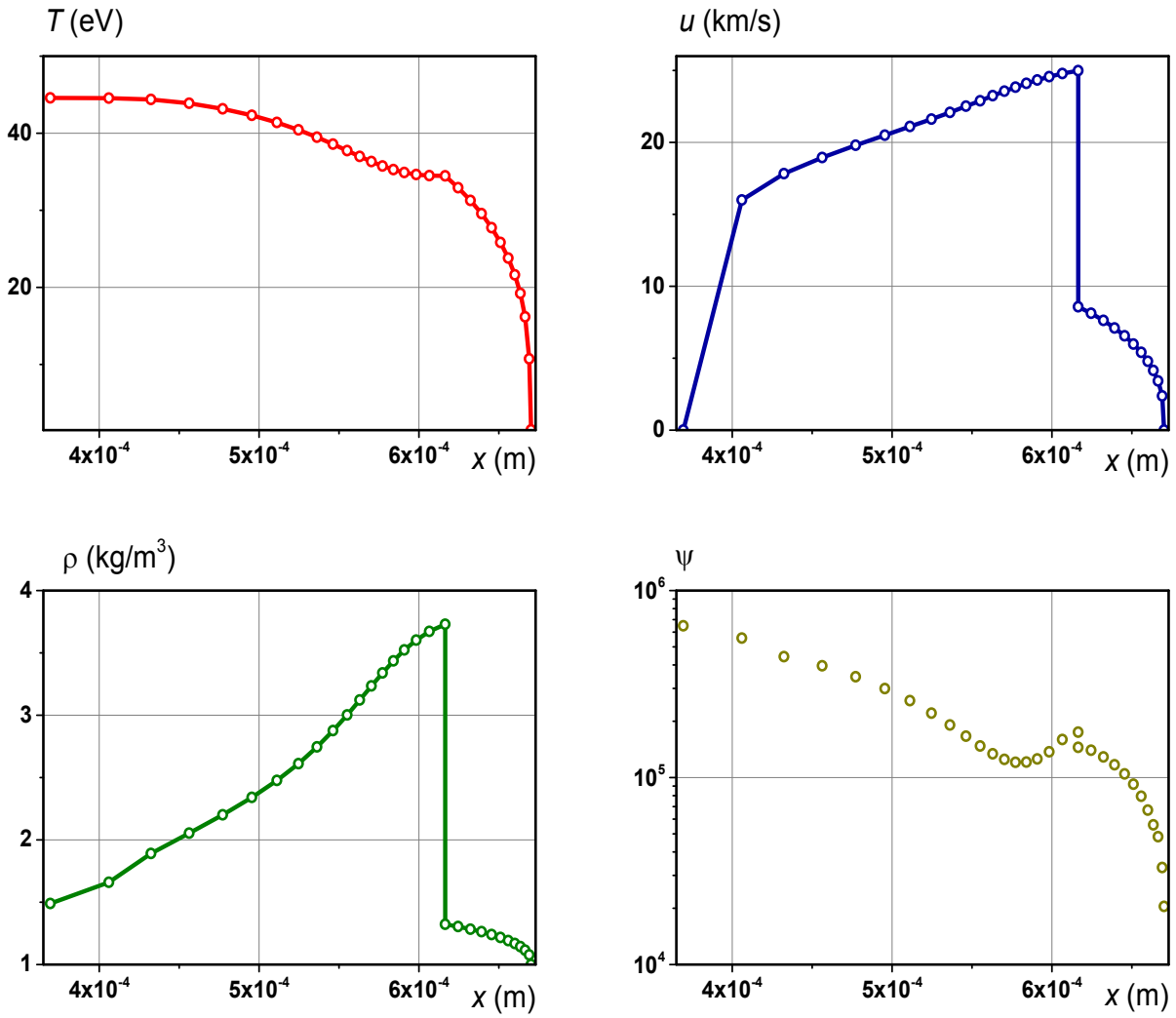

Fig. 7. Supersonic mode with λ_o= 50 at the moment t = 20 ns.

Features of the dynamic adaptation. From the point of view of constructing computational grids with dynamic adaptation brief analysis of subsonic and supersonic modes, Fig. 4-9 allows emphasizing the following features. Both modes are characterized by three moving boundaries: the front of the plasma torch with known law of motion (2.3), the shock front (strong discontinuity) and the front of the supersonic temperature wave (weak discontinuity) propagating on the temperature background, the laws of motion are unknown and must be determined during solving. All three moving boundaries explicitly allocated.

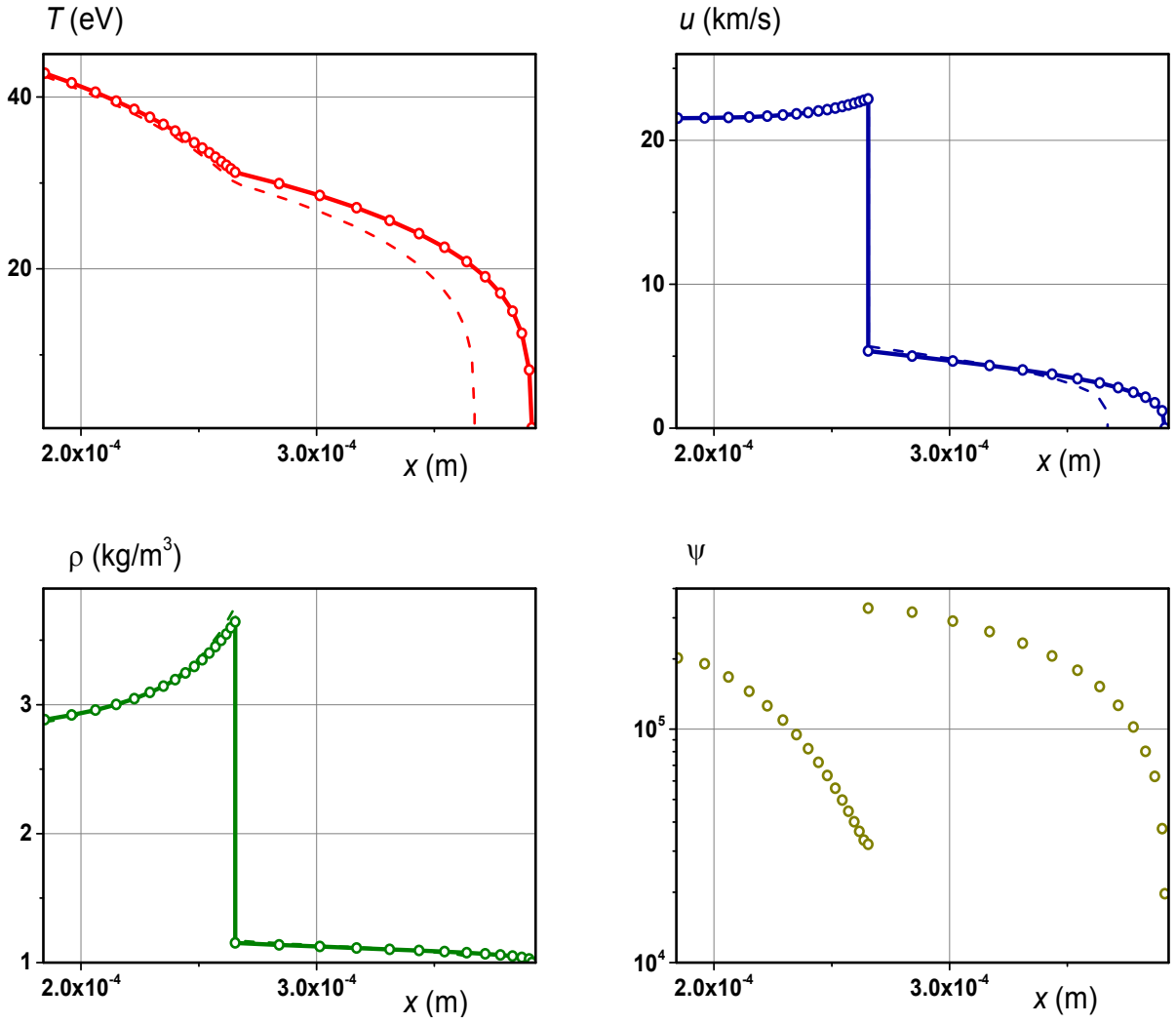

Fig. 8. Supersonic mode with λ_o= 200 at the moment t = 10 ns.

Explicit allocation of boundary of the plasma torch and of front of supersonic temperature wave allows to exclude from consideration the field of trivial solution. This is especially true in non-stationary problems, such as problems of the propagation of waves in which perturbation born near one of the boundaries and extends toward the other. At a long time of

consideration perturbation covers an area the size of which can be several orders of magnitude different from the size of the originally specified area. In such situations, the exclusion from consideration areas not covered by perturbation, plays an important role and allows you to build cost-effective computational algorithms.

Explicit allocation of the shock wave front allows to solve problems associated with discontinuous solutions.

Except to moving boundaries problem of propagation of temperature waves include several areas of rapid changing in all functions of the solution: temperature, density and velocity. In supersonic two areas, in subsonic - three.

Thus, the dynamic adaptation should take into account behavior of all functions: temperature, speed and density, and the presence of moving boundaries. Control function Q (6.1) satisfies all these requirements.

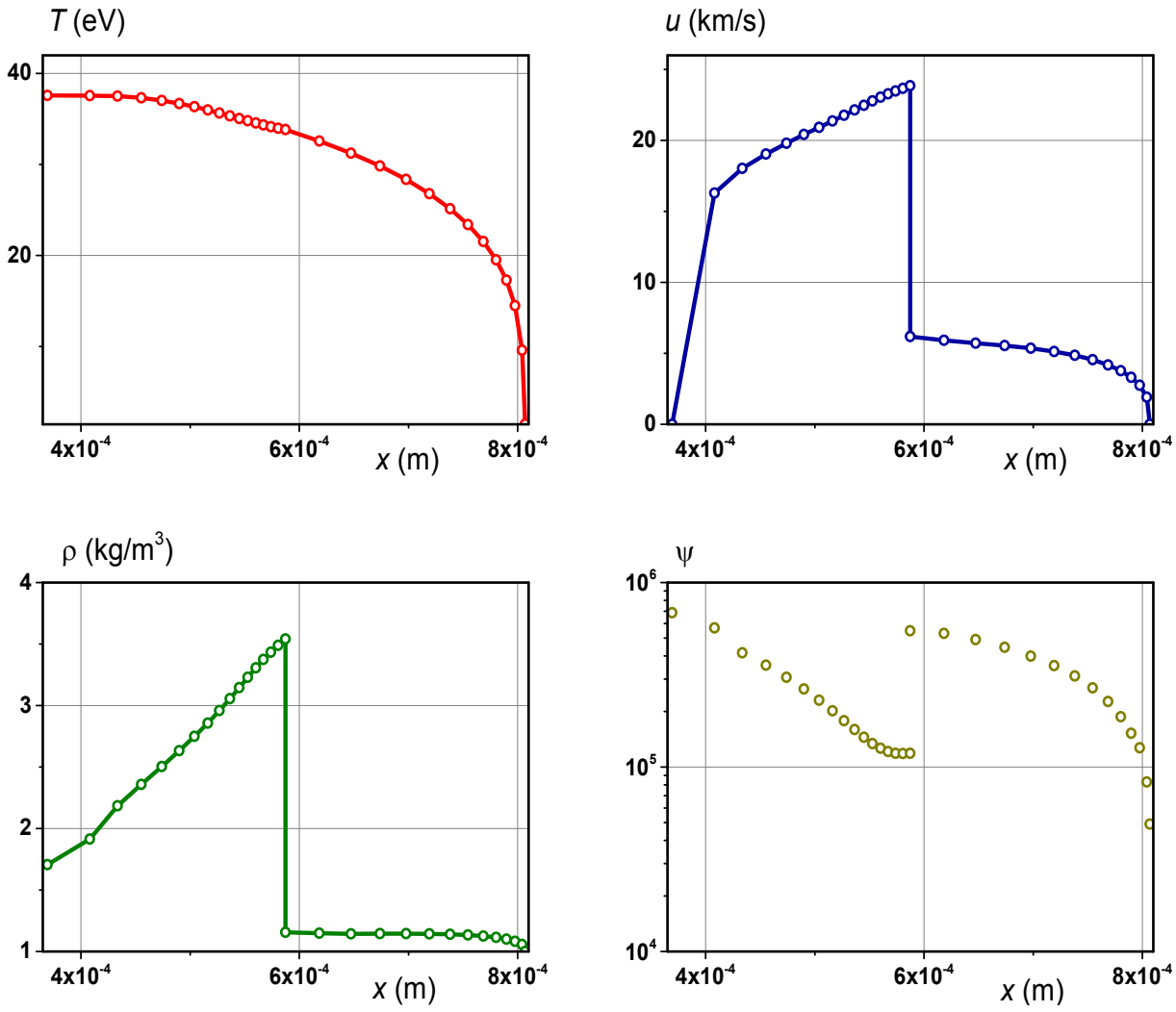

Fig. 9. Supersonic mode with λ_o= 200 at the moment t = 20 ns.

7 CONCLUSION

Simulations have shown that the dynamic characteristics of the laser plasma substantially related to the degree of nonlinearity of the thermal processes. The main features of solution of the hydrodynamic equations with nonlinear thermal conductivity include: the presence of three moving boundaries and, depending on the studied mode, two (supersonic) or three (subsonic) region of rapid changing of all functions of solution. All moving boundaries explicitly allocated. For two of them - the shock wave front and the front of the supersonic temperature wave, the law of motion is not known beforehand and determined during solving.

On an example of the problem under consideration of laser plasma spread showed the effectiveness and applicability of the proposed for solving the dynamic adaptation method. For studied problem was used adaptation function, which controls the distribution of grid nodes, depending on the features of solution. The control function has complicated form and consists of several terms. One part of them is determined from diffusion approximation and takes into account changes in the size of the area under the influence of the front of the plasma torch and of propagation of the weak and strong discontinuities. Another part of the terms defined from the principle of quasistationarity and carries out condensation of nodes of the computational grid in the areas of high gradients of temperature, density and velocity.

Application of the dynamic adaptation method allows to obtain numerical solutions on grids with an unusually small number of nodes. All calculations use the grids with the total number of nodes N=30, despite an increase of the calculation area of more than 5 orders of magnitude.

The work was supported by the RSF (project 15-11-00032).

REFERENCES

[1] D. B. Chrisey and G. K. Hubler, *Pulsed Laser Deposition of Thin Films,* John Wiley & Sons, New York (1994).

[2] A. W. Miziolek and V. Palleschi, I. Schechter, *Laser-Induced Breakdown Spectroscopy (LIBS): Fundamentals and Applications,* Cambridge University Press, Cambridge UK (2006).

[3] J. P. Singh and S. N. Thakur, *Laser-Induced Breakdown Spectroscopy,* Elsevier, Amsterdam (2007).

[4] R. E. Russo, X. Mao, O. V. Borisov and H. Liu, "Influence of wavelength on fractionation in laser ablation ICP-MS", *Journal of Analytical Atomic Spectrometry,* **15**, 1115-1120 (2000).

[5] K. F. Al-Shboul, S. S. Harilal and A. Hassanein, " Spatio-temporal mapping of ablated species in ultrafast laser-produced graphite plasmas", *Appl. Phys. Lett.* **100**, 221106 (1-4) (2012).

[6] A. Mene´ndez-Manjo´n, S. Barcikowski, G. A. Shafeev, V. I. Mazhukin and B. N. Chichkov, “Influence of beam intensity profile on the aerodynamic particle size distributions generated by femtosecond laser ablation”, *Laser and Particle Beams,* **28**, 45–52 (2010).

[7] J. R. Freeman, S. S. Harilal and A. Hassanein, “Enhancements of extreme ultraviolet emission using prepulsed Sn laser-produced plasmas for advanced lithography applications”, *J. Appl. Phys.* **110**(8), 083303 (1-8) (2011).

[8] M. Shahzad, O. Culfa, A. K. Rossall, L. A. Wilson, O. Guilbaud, S. Kazamias, O. Delmas, J. Demailly, A. Maitrallain, M. Pittman, E. Baynard, M. Farjardo and G. J. Tallents, “Diagnosis of energy transport in iron buried layer targets using an extreme ultraviolet laser”, *Phys. Plasmas,* **22**, 023301 (1-11) (2015).

[9] C. Chenais-Popovics, O. Rancu, P. Renaudin and J. C. Gauthier, "X-Ray Spectroscopy of Laser-Produced Hot Dense Plasmas", *Physica Scripta,* **65**, 163-167 (1996).
[10] X. Zeng, X. Mao, S. S. Mao, J. H. Yoo, R. Greif and R. E. Russo, "Laser–plasma interactions in fused silica cavities", *J. Appl. Phys,* **95**(3), 816–822 (2004).
[11] V. I.Mazhukin, I. Smurov and G. Flamant, "2D-simulation of the system: laser beam + laser plasma + target", *J. Applied Surface Science,* **96-98**, 89-96 (1996).
[12] Sy-Bor Wen, X. Mao, C. Liu, R. Greif and R. Russo, "Expansion and radiative cooling of the laser induced plasma", *Journal of Physics: Conference Series,* **59**, 343–347 (2007).
[13] V. I.Mazhukin, I. Smurov and G. Flamant, "Simulation of Laser Plasma Dynamics: Influence of Ambient Pressure and Intensity of Laser Radiation", *J. Comp. Phys,* **112**(20), 78-90 (1994).
[14] S. Panchatsharam, Bo Tan and K. Venkatakrishnan, "Femtosecond laser-induced shockwave formation on ablated silicon surface", *J. Appl. Phys,* **105**, 093103 (2009).
[15] S. S. Harilal, G. V. Miloshevsky, P. K. Diwakar, N. L. LaHaye and A. Hassanein, "Experimental and computational study of complex shockwave dynamics in laser ablation plumes in argon atmosphere", *Physics of Plasmas,* **9**, 083504 (1-11) (2012).
[16] O. Benavides, L. de la Cruz May, A. Flores Gil and J.A. Lugo Jimenez, "Experimental study on reflection of high-intensity nanosecond Nd:YAG laser pulses in ablation of metals", *Optics and Lasers in Engineering,* **68**, 83–86 (2015).
[17] V. I. Mazhukin, V. V. Nossov and I. Smurov, "Modeling of plasma-controlled evaporation and surface condensation of Al induced by 1.06 and 0.248 m laser radiations", *J. Appl. Phys.,* **101**(2), 024922 – 024937 (2007).
[18] A. E. Hussein, P. K. Diwakar, S. S. Harilal and A. Hassanein, "The role of laser wavelength on plasma generation and expansion of ablation plumes in air", *J.Appl. Phys,* **113**, 143305 (1-11) (2013).
[19] K.-H. Leitz, B. Redlingshöfer, Y. Reg, A. Otto and M. Schmidt, "Metal Ablation with Short and Ultrashort Laser Pulses", *Physics Procedia,* **12**, 230–238 (2011).
[20] V. Morel, A. Bultel, J. Annaloro, C. Chambrelan, G. Edouard and C. Grisolia, "Dynamics of a fs/ps laser-induced aluminum plasma out of thermodynamic equilibrium in a nitrogen background gas", *Spectrochimica Acta Part B,* **103–104**, 112–123 (2015).
[21] N. G. Basov, V. A. Boiko, O. N. Krokhin, O. G. Semenov and G. V. Sklizkov, "Reduction of reflection coefficient for intense laser radiation on solid surfaces", *Sov Phys - Tech Phys,* **13**, 1581–2 (1969).
[22] V. I. Mazhukin, A. A. Uglov and B. N. Chetverushkin, "Low-temperature laser plasma near metal surfaces in the high-pressure gases. A Review", *Kvantovaya elektronika,* **10**(4), 679-701 (1983).
[23] A. Miloshevsky, S. S. Harilal, G. Miloshevsky and A. Hassanein. "Dynamics of plasma expansion and shockwave formation in femtosecond laser ablated aluminum plumes in argon gas at atmospheric pressures", *Physics of Plasmas,* **21**, 043111 (1-11) (2014).
[24] V. I. Mazhukin, A. V. Mazhukin and M. G. Lobok, "Comparison of Nano- and Femtosecond Laser Ablation of Aluminium", *Laser Physics,* **19**(5), 1169 – 1178 (2009).
[25] M. R. Kasaai, V. Kacham, F. Theberge and S. L. Chin, "The interaction of femtosecond and nanosecond laser pulses with the surface of glass", *J. Non-Cryst. Solids,* **319**(1-2), 129–135 (2003).
[26] A. Semerok and C. Dutouque, "Analytical performances of laser-induced micro-plasma of Al samples with single and double ultrashort pulses in air and with Ar-jet: A comparative study", *Spectrochimica Acta Part B,* **99**, 163–171 (2014).
[27] N. A. Inogamov, V. V. Zhakhovsky, Yu. V. Petrov, V.A. Khokhlov, S. I. Ashitkov,K.V. Khishchenko, K. P. Migdal, D. K. Ilnitsky, Yu. N. Emirov, P. S. Komarov, V. V. Shepelev,C. W. Miller, I. I. Oleynik, M. B. Agranat, A. V. Andriyash, S. I. Anisimov, and V. E .Fortov.

"Electron-Ion Relaxation, Phase Transitions, and Surface NanoStructuring Produced by Ultrashort Laser Pulses in Metals", *Contrib. Plasma Phys,* **53**(10), 796 – 810 (2013).
[28] C. Wu and L. V. Zhigilei, "Microscopic mechanisms of laser spallation and ablation of metal targets from large-scale molecular dynamics simulations", *Appl. Phys. A,* **114**, 11–32 (2014).
[29] V. I. Mazhukin, M. M. Demin and A. V. Shapranov, "High-speed laser ablation of metal with pico- and subpicosecond pulses", *Applied Surface Science,* **302**, 6–10 (2014).
[30] V. I.Mazhukin, A. A. Samokhin, M. M.Demin and A. V.Shapranov, "Modeling of nanosecond laser vaporization and explosive boiling of metals", *Mathematica Montisnigri,* **29**, 68 – 90 (2014).
[31] V. I.Mazhukin, A. A. Samokhin, A. V.Shapranov and M. M.Demin, "Modeling of thin film explosive boiling - surface evaporation and electron thermal conductivity effect", *Mater. Res. Express,* **2**(1), 016402, 1-9 (2015).
[32] A. R. Casavola, G. Colonna and M. Capitelli, "Kinetic model of titanium laser induced plasma expansion in nitrogen environment", *Plasma Sources Sci. Technol,* **18**, 025027, 1-8 (2009).
[33] D. Autrique, V. Alexiades and H. Khanal, "Hydrodynamic modeling of ns-laser ablation", *Electronic Journal of Differential Equations, Conference on Differential Equations and Computational Simulations,* **20**, 1-14 (2013).
[34] A. A. Samarskii and I. M. Sobol', "Examples of numerical calculations of thermal waves", *Zh. Vychisl. Mat. Mat. Fiz.,* **3**(4), 703 -719 (1963).
[35] P. P. Volosevich, S. P. Kurdyumov and E. I. Levanov, "Various Heating Regimes in the Interaction of Intense Radiation Fluxes with Matter", *Prikl. Mekh. Tekh. Fiz.*, **5**, 41–48 (1972).
[36] P. P. Volosevich and E. I. Levanov, *Self-Similar Solutions of Problems in Gas Dynamics and Hear Transfer,* MFTI, Moscow, (1997).
[37] Ya. B. Zel'dovich and Yu. P. Raizer, *Physics of shock waves and high-temperature hydrodynamic phenomena,* Academic Press, New York, (1966-1967).
[38] P. V. Breslavskii and V. I. Mazhukin, "Dynamic Adaptation Method in Gas Dynamics Simulations", *Mat. Model,*. **7**(12), 48–78 (1995).
[39] V. I. Mazhukin, M. M.Demin, A. V.Shapranov and I. Smurov, "The method of construction dynamically adapting grids for problems of unstable laminar combustion", *Numerical Heat Transfer, Part B: Fundamentals,* **44**(4), 387 – 415 (2003).
[40] A. V. Mazhukin and V. I. Mazhukin, "Dynamic Adaptation for Parabolic Equations", *Comp. Math. Math. Phys.,* **47**(11), 1833 – 1855 (2007).
[41] P. V. Breslavskii and V. I. Mazhukin, "Dynamically Adapted Grids for Interacting Discontinuous Solutions", *Comp. Math. Math. Phys.,* **47**(4), 687 – 706 (2007).
[42] P. V. Breslavskii and V. I. Mazhukin, "Dynamic Adaptation Method in Gasdynamic Simulations with Nonlinear Heat Conduction", *Comp. Math. Math. Phys.,* **48**(11), 2102 – 2115 (2008).

The results were presented at the thirteenth international seminar "Mathematical models & modeling in laser-plasma processes & advanced science technologies" (May 30 - June 6, 2015, Petrovac, Montenegro).